Korean J. Chem. Eng., 39(4), 913-919 (2022)
DOI: 10.1007/s11814-021-0977-z

pISSN: 0256-1115
eISSN: 1975-7220

Facile construction of a $Bi_6O_6(OH)_3(NO_3)_3 \cdot 1.5H_2O/Bi_2O_2CO_3$ heterojunction with enhanced photocatalytic degradation activity

Huilan Ye*, Yiting Wu*, Ziqing Zhong*, Shichang Sun*, Jia Chen, Weiming Zhou*, Ibrahim Lawan***, Liwei Wang****,†, and Zhanhui Yuan*,†**

*College of Materials Engineering, Fujian Agriculture and Forestry University, Fuzhou, 350002, China
**College of Mechanical and Electrical Engineering, Fujian Agriculture and Forestry University, Fuzhou, 350002, China
***Department of Agricultural and Environmental Engineering, Bayero University Kano, Nigeria
****Ocean College, Minjiang University, Fuzhou 350108, China
(*Received 23 June 2021 • Revised 29 September 2021 • Accepted 6 October 2021*)

Abstract−A $Bi_6O_6(OH)_3(NO_3)_3 \cdot 1.5H_2O$ (BBN)/$Bi_2O_2CO_3$ (BOC) heterojunction was designed for the first time via a facile hydrothermal method. The photocatalytic performance of catalysts was evaluated by degrading Rhodamine B (RhB) under simulated solar light irradiation. It was found that the degradation rate of RhB by 25 wt%BBN/BOC was dramatically increased about 1.5 and 4.7 times compared with that of pure BOC and BBN, respectively. The enhanced photocatalytic performance migth be attributed to the effective separation of photoinduced electron-hole pairs, benefiting from the construction of heterojunction. Furthermore, the mechanism upon BBN/BOC composites photocatalyst was investigated, expecting this work will bring new insight into the theoretical study and application of semiconductors materials.

Keywords: $Bi_6O_6(OH)_3(NO_3)_3 \cdot 1.5H_2O$, $Bi_2O_2CO_3$, Heterojunction, Semiconductors, Composite Materials

INTRODUCTION

Increasingly serious water pollutants have threatened the balance of the ecological environment, making it is urgent to develop a fast and effective water treatment technology [1,2]. Photocatalytic technology, with the advantage that can achieve complete degradation of dyes, has been considered as one of the advanced environmental purification technologies [3]. However, several disadvanteges of single-component semiconductor photocatalysts, such as poor visible light absorbtion, rapid recombination of photoinduced electrons (e^-) and holes (h^+), limits the application of photocatalytic materials [4]. Therefore, various ways have been adopted to improve the photocatalytic performance of semiconductor photocatalyst, such as ion doping [5], heterojunction [6], and coupling with conductive materials [7]. Among them, construction heterojunction has been confirmed to be an available approach in overcoming the drawbacks of single-component photocatalysts. Lu et al. [8] reported that Bi_2O_3/Bi_2SiO_5 heterojunction improved its photocatalytic performance, which benefited from the effective separation of photogenerated e^--h^+ pairs at the heterojunction interface. Kong et al. [9] also synthesized $BiFeO_3$-$(Bi/Fe)_2O_3$ heterojunction with high-efficiency photocatalytic destruction of gaseous toluene.

Recently, bismuth subcarbonate ($Bi_2O_2CO_3$, BOC) has received a large consideration to act as a photocatalyst. BOC has a unique layered structure which facilitates the transmission of photo-generated electrons [10]. Furthermore, it is non-tox and chemically stable, and belongs to environmentally friendly material [11]. At present, a large number of papers have been published on the heterojunction between BOC and narrow-band gap semiconductors [12], but the limited number of narrow-band gap semiconductors restricts the further application of BOC to some extent. So far, little has been reported about the recombination between BOC and wideband gap semiconductors. Similar to BOC, bismuth subnitrate ($Bi_6O_6(OH)_3(NO_3)_3 \cdot 1.5H_2O$, BBN), also as a member of bismuth-based semiconductors, was stacked by $(Bi_2O_2)^{2+}$, OH^- and $(NO_3)^-$ layers, which may decrease the probability of lattice mismatch with BOC [13]. In addition, considering that the band-gap structure of BBN is matched with that of BOC, we designed the BBN/BOC heterojunction to facilitate the separation of photogenerated carriers and thus improve the photocatalytic efficiency of single-component photocatalysts. Furthermore, at present, there are no studies reported on enhancing photocatalyst performance by constructing BBN/BOC heterojunction.

Here, a simple two-step hydrothermal process was used to synthesize the composite BBN/BOC, and its photocatalytic activity was evaluated by degrading RhB under simulated solar irradiation. The mechanism of the enhancement of the photocatalytic activity at the heterojunction interface was discussed in detail. This study could provide data and theoretical support for the design of bismuth series photocatalysts and lay a foundation for the further application of photocatalysts.

EXPERIMENTAL

1. Materials

All the chemical reagents are of analytical grade and used with-

†To whom correspondence should be addressed.
E-mail: wlw@mju.edu.cn, zhanhuiyuan@fafu.edu.cn

out further purification. Sodium hydroxide (NaOH), Na_2CO_3 and sodium sulfate (Na_2SO_4) were purchased from Xilong Scientific, China. Ethanol and Bismuth nitrate ($Bi(NO_3)_3{\cdot}5H_2O$), thylenediamine tetraacetic acid (EDTA), isopropanol (IPA) and benzoquinone (BQ) were purchased from Shanghai Macklin Biochemical Co., Ltd, China. Deionized (DI) water is used throughout the process.

2. Synthesis of BBN

In the process of synthesizing BBN, 1 mmol $Bi(NO_3)_3{\cdot}5H_2O$ and 40 ml DI water were put in a beaker with magnetic stirring for 20 min. Then, the homogeneous solution was poured into a 30 ml stainless steel autoclave with Teflon lined and heated to 180 °C for 24 h. After naturally cooled to room temperature, the sample was collected by washing with water and anhydrous ethanol 3-5 times, and drying at 70 °C for 8 h in a vacuum oven.

3. Synthesis of BOC, BBN/BOC

BOC, BBN/BOC were both synthesized by a simple hydrothermal method. In a typical synthesis, 1 mmol $Bi(NO_3)_3{\cdot}5H_2O$ was added into the beaker with 40 ml DI water to form a solution with magnetic stirring for 10 min, and then Na_2CO_3 solution was added drip by drip with continued stirring until the pH was adjusted to nearly 8 at room temperature. Then, a certain amount of BBN was added. The mixed solution was transferred to a 50 ml stainless steel autoclave with Teflon lined and heated to 180 °C for 12 h. After naturally being cooled to room temperature, the synthetic samples were washed 3-5 times with DI water and ethanol, respectively, and dried in a vacuum oven at 70 °C for 8 h. Samples synthesized with different concentrations of BBN were recorded as BOC, 15 wt%BBN/BOC, 25 wt%BBN/BOC, 30 wt%BBN/BOC, 50 wt%BBN/BOC, 60 wt%BBN/BOC, respectively.

4. Characterization

The crystal structure of the samples was determined by X-ray diffractometer (Bruker D8 Advance), using monochromatized Cu-Kα radiation in the 2θ value range of 5-80° operated at 40 kV and 30 mA. The surface morphology of the samples was stdied by scanning electron microscopy (Hitachi Regulus 8100). The X-ray photoelectron spectroscopy (XPS) data was obtained by AXISULTRA DLD-600W (Kratos, Japan) using a monochromatic Al Kα X-ray source (h=1486.6 eV) operating at 150 W, and all the binding energy values were calibrated by using the reference of C1s=284.8 eV. Ultraviolet-visible diffuse reflection (UV-Vis DRS) spectrum was measured with a Shimadzu UV 2600 ultraviolet-visible spectrophotometer using $BaSO_4$ as a reference. Transient photocurrent responses, electrochemical impedance spectra (EIS) and Mott-Schottky test, a platinum plate serving as the counter electrode and an Ag/AgCl (saturated KCl) (SCE) served as a reference electrode, were recorded by the combination of an electrochemical workstation (CS310H) and a 250 W xenon lamp (FX300r). A quartz cell was used as reactor for photocurrent test in which 100 mL 0.5 M Na_2SO_4 solution was placed.

5. Evaluation of Photocatalytic Degradation Performance

The photocatalytic performance of samples was characterized by degrading organic dyes RhB solution. 20 mg photocatalyst was dispersed into a 100 mL aqueous solution of RhB (10 mg/L), agitating for 25 min in the dark to reach the adsorption-desorption equilibrium. Afterward, under the continuous irradiation of 250 W Xenon lamps and constant magnetic stirring, the photocatalytic degradation was carried out at room temperature; about 3 ml of the solution was taken out every 5 min. After the photocatalyst was removed by centrifugation, the absorbance of the reaction solution was measured on a UV-vis spectrophotometer (Shimadzu UV 2600) at λ= 554 nm. The degradation efficiency of RhB can be derived according to $D\%=(C_0-C_t)/C_0\times100\%$, where C_0 and C_t are the initial and residual RhB concentration, respectively. Ethylenediamine tetraacetic acid (EDTA), isopropanol (IPA) and benzoquinone (BQ) were used as trapping agents to detect free radicals such as h^+, $\bullet O_2^-$ and •OH.

RESULTS AND DISCUSSION

1. Structure and Morphology

X-ray diffraction (XRD) was used to characterize the composition of the as-prepared samples. The XRD patterns of BOC, BBN and a series of BBN/BOC are presented in Fig. 1. It can be seen that the typical peaks at 12.93°, 23.90°, 26.03°, 30.25°, 32.72°, 42.29°, 52.23°, 56.89° showed in the pattern of BOC, corresponding to the (002), (011), (004), (013), (110), (114), (116), (123) crystal planes of BOC (JCPDS: 041-1488), respectively. The main diffraction peaks of BBN attributed to the (002), (102), (006) and (200) facets are detected at 2θ=10.32°, 25.54°, 31.30° and 47.62°, respectively. It is in good agreement with the phase of BBN (JCPDS: 053-1038). Comparison to BBN and BOC, the XRD patterns consist of BBN and BOC phases in the as-prepared BBN/BOC, and no other impurity peaks are detected in these photocatalysts. This result unambiguously proves that the BBN/BOC was mainly composed of BOC and BBN.

The SEM images were adopted to observe the general morphologies of BBN, BOC and 25 wt%BBN/BOC composite. As shown in Fig. 2(a), the pristine BBN was composed of irregularly shaped particles. And the BOC was 3D pine-like structure assembled by 2D nanosheets in Fig. 2(b). However, in BBN/BOC composite (Fig. 2(c)-(d)), the morphology of BOC turned from 3D pine-like structure to 3D flower structure, and BBN was perfectly attached to the BOC. Interestingly, compared with BOC, the sheet is thinner, which may be due to the introduction of BBN in the synthesis process, thus affecting the morphology of BOC. And the changes of the

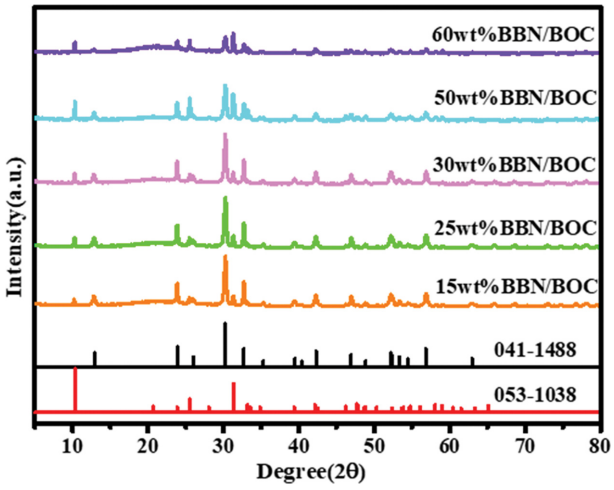

Fig. 1. The XRD patterns of BOC, BBN, and BBN/BOC composites.

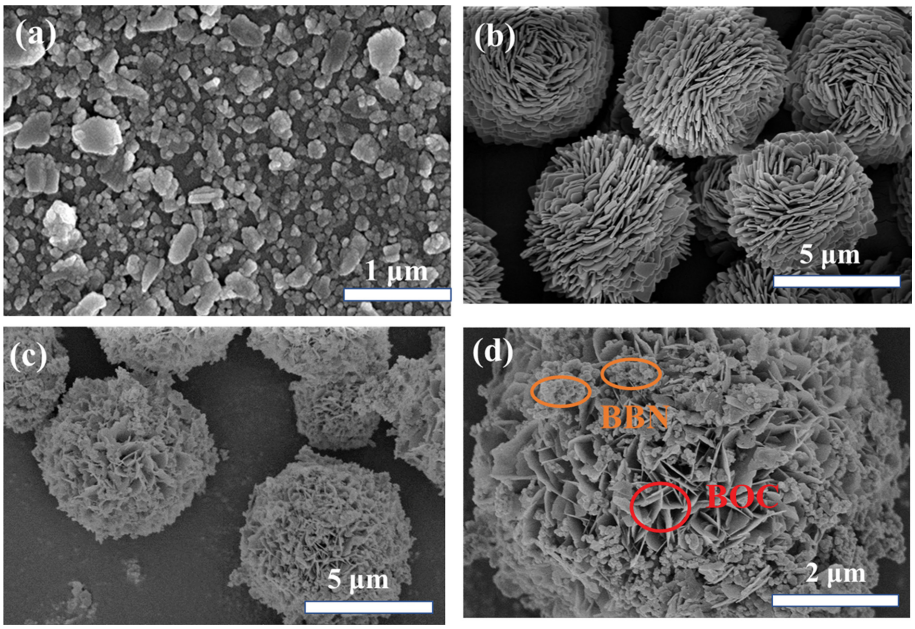

Fig. 2. The SEM image of BBN (a), BOC (b) and 25 wt%BBN/BOC (c)-(d).

morphology and thickness of the as fabricated samples indicate that BBN plays a pivotal role in controlling the morphology. Besides, the thin nanosheets mutual staggering can offer large specific surface area for mass transfer as well as supply more active sites.

The surface chemical composition and state of the BOC and 25 wt%BBN/BOC samples were studied by XPS. Fig. 3(a) is the survey spectrum of the BOC and 25 wt%BBN/BOC; it is obvious that Bi, O, C, and N elements were found in sample 25 wt%BBN/BOC, whereas N elements were not found in BOC. In Fig. 3(b), the two obvious peaks at 157.65 eV and 162.8 eV belong to the orbital $4f_{7/2}$ and $4f_{5/2}$ of Bi^{3+} in BOC, respectively. Moreover, the two obvious peaks at 158.81 eV and 164.17 eV belong to the orbital $4f_{7/2}$ and $4f_{5/2}$ of Bi^{3+} in 25 wt%BBN/BOC composite, respectively. The shift of the feature peak position of Bi^{3+} might be attributed to the interaction between BOC and BBN [14]. In Fig. 3(c), the O1s peak of BOC at 528.8 and 529.98 eV was related to the O^{2-} and Bi-O in BOC [15]. In the O1s spectrum of 25 wt%BBN/BOC, the peak at 529.56 eV belongs to Bi-O in BOC and BBN, the peak at 531.3 eV is associated with the O^{2-} in 25 wt%BBN/BOC composite [16], and the peaks at 531.3 eV is the typical peak of O_2 on the surface of BBN/BOC composites compared with that of BOC. The O_2 on the surface of BBN/BOC composites is beneficial to the generation of O^{2-} with strong oxidation, thus improving the photocatalytic performance of BBN/BOC. Fig. 3(d) is the narrow spectrum of C1s in BOC and 25 wt%BBN/BOC. For BOC, two peaks are observed at 284.8 eV and 287.9 eV, which can be attributed to the adventitious carbon and carbonate [17]. While the peak at 287.9 eV ascribed to carbonate ion in BOC was shifted up to 288.9 eV after coupling with BBN, proving that there is a strong interaction between BOC and BBN, which led to alternate the distribution of the electric charge of C atoms in the composite [18]. Fig. 3(e) is the narrow spectrum of N1s in sample BBN/BOC composite, which corresponds to NO_3^- of BBN at 406.42 eV [13], indicating the BBN/BOC composite is composed of BOC and BBN.

2. Photocatalytic Activity

RhB was selected as a reference to evaluate the photocatalytic performance of composites BBN/BOC under simulated sunlight. Before light irradiation, the mixed solution of RhB and photocatalyst was stirred in the dark for 25 min to reach the adsorption-desorption equilibrium. Fig. 4(a) displays the photodegradation efficiency of RhB as a function of irradiation time over the as-prepared samples, where C_0 is the initial concentration of RhB, and C_t is the concentration of remaining RhB at different irradiation times. And X-axis represents photocatalytic reaction time, '0 min' represents the boundary among dark condition and in light condition, and is marked by the vertical dotted line. The left side of the dotted line is the treatment time in the dark, and the right side of the dotted line is the reaction time under similated light irradiation [19-22]. As shown in Fig. 4(a), when BBN was added to the degradation system, only 40% of RhB was degraded in 25 minutes due to the wide bandgap of BBN. Compared with BBN, the degradation rate of BOC is about 80% under the same conditions. However, in BBN/BOC composites, with the increase of BBN content, the degradation activity increased significantly, but when the content of BBN increased to 50%, the activity decreased, which may be because BBN became the capturing center of electrons and holes, leading to the recombination of e^- and h^+. To reduce the error caused by the operation process, the photocatalytic degradation performance of each sample was analyzed through repeated experiments, obtaining the error bar curve from the experimental results (Fig. 4(a)). It is obvious that 25 wt%BBN/BOC heterojunction composites showed the highest photocatalytic performance with the RhB degradation ratio of 99.7% under the same consideration.

To further understand the photocatalytic efficiency of the samples, the pseudo-first-order kinetic equation curve of the RhB decomposition over prepared composites was investigated. The pseudo-

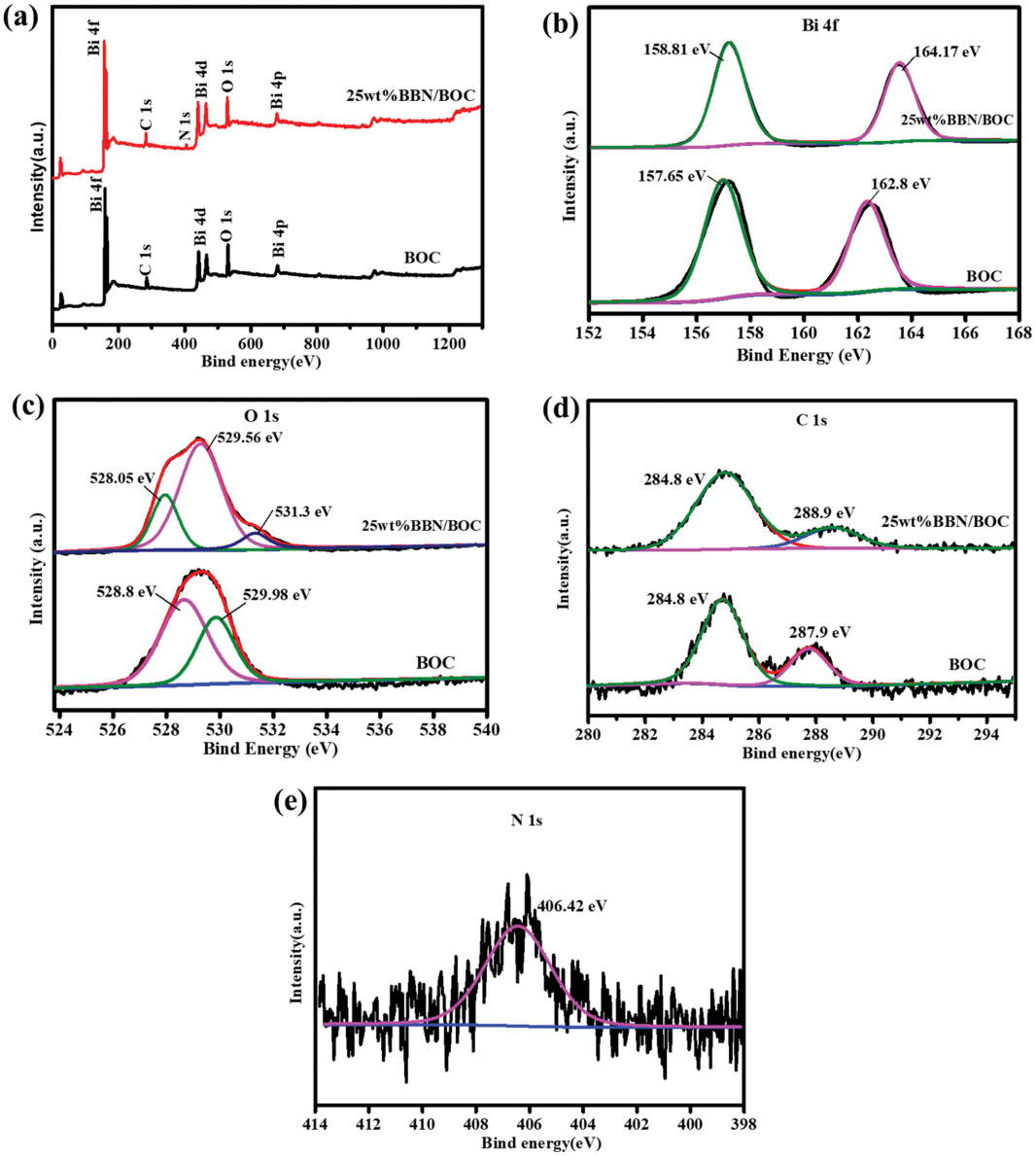

Fig. 3. XPS spectra of BOC and the 25 wt% BBN/BOC composite: (a) Survey of the sample, (b) Bi 4f, (c) O 1s, (d) C 1s, (e) N 1s.

first-order kinetics equation is expressed as $\ln(C_t/C_0)=k_{app}t$, where k_{app} is the apparent pseudo-first-order kinetic constant (min^{-1}). The relationships between $\ln(C_t/C_0)$ and irradiation time (t) of BOC, and BBN/BOC composites are plotted in the insets of Fig. 4(b). The excellent fitting indicates that the photoreaction follows the first-order reaction kinetics. As shown in Fig. 4(b), the value of k for BOC, BBN, 15 wt%BBN/BOC, 25 wt%BBN/BOC, 30 wt%BBN/BOC, 50 wt%BBN/BOC and 60 wt%BBN/BOC was 0.06657, 0.02197, 0.07197, 0.10452, 0.08449, 0.05151, 0.04434 min^{-1}, respectively, calculating that the photocatalytic activity of 25 wt%BBN/BOC composite is 1.5, 4.7 times than pure BOC and BBN. In addition, the composites of BBN/BOC possess better photocatalytic performance than other composites in published papers as displayed in Table S1. Furthermore, reproducibility and stability are important to photocatalysts for potential applications. To examine photocatalytic stability, cycling runs for the photocatalytic degradation of RhB with the BBN/BOC composites were performed under the same conditions. As shown in Fig. 4(c), it is the relationship between RhB degradation ratio and cycling times. BBN and BOC, as well as 15 wt%BBN/BOC, 25 wt%BBN/BOC and 30 wt%BBN/BOC with good photocatalytic activity were selected for cyclic tests. After undergoing four repeated runs, the photocatalytic activity of pure samples BBN and BOC gradually decreased, while the stability of the other photocatalysts with different proportions all showed a good stability. Especially 25 wt%BBN/BOC, after four cycles, the photocatalytic degrading RhB activity of the composite remained stable with only 0.39% reduction, illustrating the 25 wt%BBN/BOC has a promising application prospect.

3. Photocatalytic Mechanism

To better understand the reasons for the improvement of the photocatalytic performance of photocatalysts, the following methods were adopted in this paper for verification. The UV-Vis diffuse

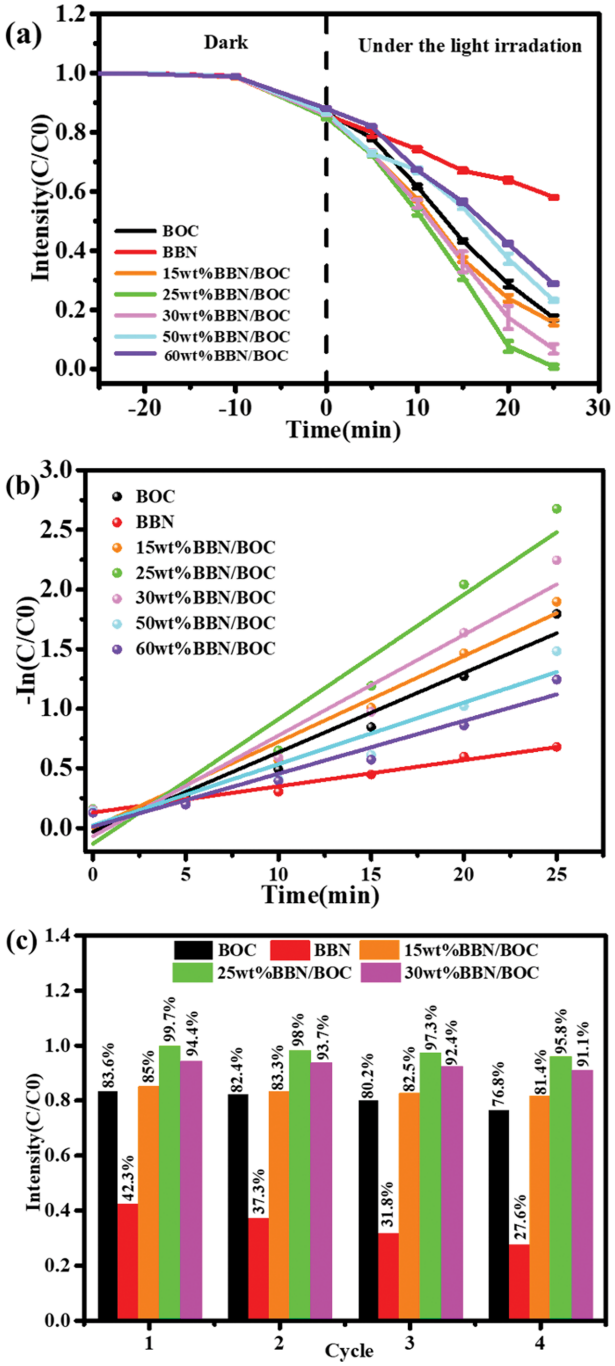

Fig. 4. The time course and the error bar curve of photocatalytic degrade RHB (a) and pseudo-first-order reaction kinetics (b) over as-prepared samples, and the cycle test curve over BBN, BOC and BBN/BOC composites (c).

reflection spectra were adopted to analyze the optional property of as-prepared BBN and BOC, as shown in Fig. 5(a). It can be observed that BOC and BBN have an absorption band with the edge at about 350 nm, corresponding to the bandgap of 3.46 eV and 3.4 eV, respectively [23]. The E_{CB} and E_{VB} of BOC are −0.2 eV and 3.2 eV, respectively. For BBN, the E_{CB}=−0.75 eV, E_{VB}=2.71 eV according to Fig. 5(b). The two semiconductors have a matching bandgap structure, which is conducive to the construction of a heterojunction interface to facilitate the transmission and movement of photoinduced e^--h^+ pairs.

To study the separation efficiency of photogenerated carriers at the interface of heterojunction, the transient photocurrent response and electrochemical impedance spectroscopy (EIS) of each sample were measured. Fig. 5(c) is the transient photocurrent time curve of each sample. After several intermittent on and off lamp irradiations, the photocurrent response intensity remained stable. In general, the higher photocurrent, the higher photoinduced charge separation and the longer lifetime of photoinduced electrons and holes [24]. As shown in Fig. 5(c), the photocurrent of 25 wt%BBN/BOC is obviously higher than that of the other catalyst, manifesting that 25 wt%BBN/BOC has the best separation of photoinduced charge carriers. The results indicate that the photoluminescent electron and hole generation and separation rate are greatly improved when BBN/BOC composites form a heterojunction. Moreover, the electrochemical impedance spectra (EIS) were used to used to further study the photoelectric chemical trends of BOC and BBN/BOC composites. The smaller the radius, the lower the resistance of charge transfer and the higher photoinduced charge separation [18,25]. As shown in Fig. 5(d), the radius of composite 25 wt%BBN/BOC was much smaller than that of pure BOC, signifying that the addition of BBN promotes the transfer of photoelectric charge and benefits the separation of photoelectric carriers, which corresponds to the results of the transient photocurrent response. Remarkably, compared with other wt%BOC/BBN composites, 25 wt%BOC/BBN exhibits the highest photocurrent response and the lowest charge transfer resistance, which might be ascribed to their own structural characteristic. It is reported that BBN is often used as an auxiliary catalyst because of its wide optical band gap and low quantum efficiency [13,14,27]. For BOC, the uneven charge distribution between the Bi-O layer and the carbonate ion layer leads to the generation of a static internal electric field (IEF), and the interlayer distance between two neighboring $[Bi_2O_2]^{2+}$ layers are larger than other semiconductor catalysts in Aurivillius family, which is beneficial to the separation of photoexcited carriers [4,17,28,29]. Therefore, BOC of BBN/BOC plays a dominant role in the photocatalytic degradation of RhB, which is consistent with the test results of photocatalysis. When the content of BBN in BBN/BOC is 25 wt%, BBN acts as a charge transfer channel to separate electron holes to the maximum extent, while preserving the photocatalytic properties of BOC. Therefore, 25 wt%BOC/BBN exhibits the highest photocurrent response and the lowest charge transfer resistance.

In general, the species and number of active species dominate the whole phototreamination degradation process. In this paper, the contribution of three active factors was studied through the capture experiment of active species, as shown in Fig. 5(e)-(f). The capture experiments of h^+, $\cdot O_2^-$ and ·OH were carried out. The selected scavengers were ethylene diamine tetra-acetic acid (EDTA), isopropanol (IPA) and benzoquinone (BQ), the blank control group was set for comparison without adding any free radical scavenger. Fig. 5(e)-(f) shows the relationship between the concentration and the degradation time of RhB. When EDTA was used as h^+ scavenger is added into the reaction system, the removal rate of RhB was sharply decreased. Compared with EDTA, when IPA and BQ were

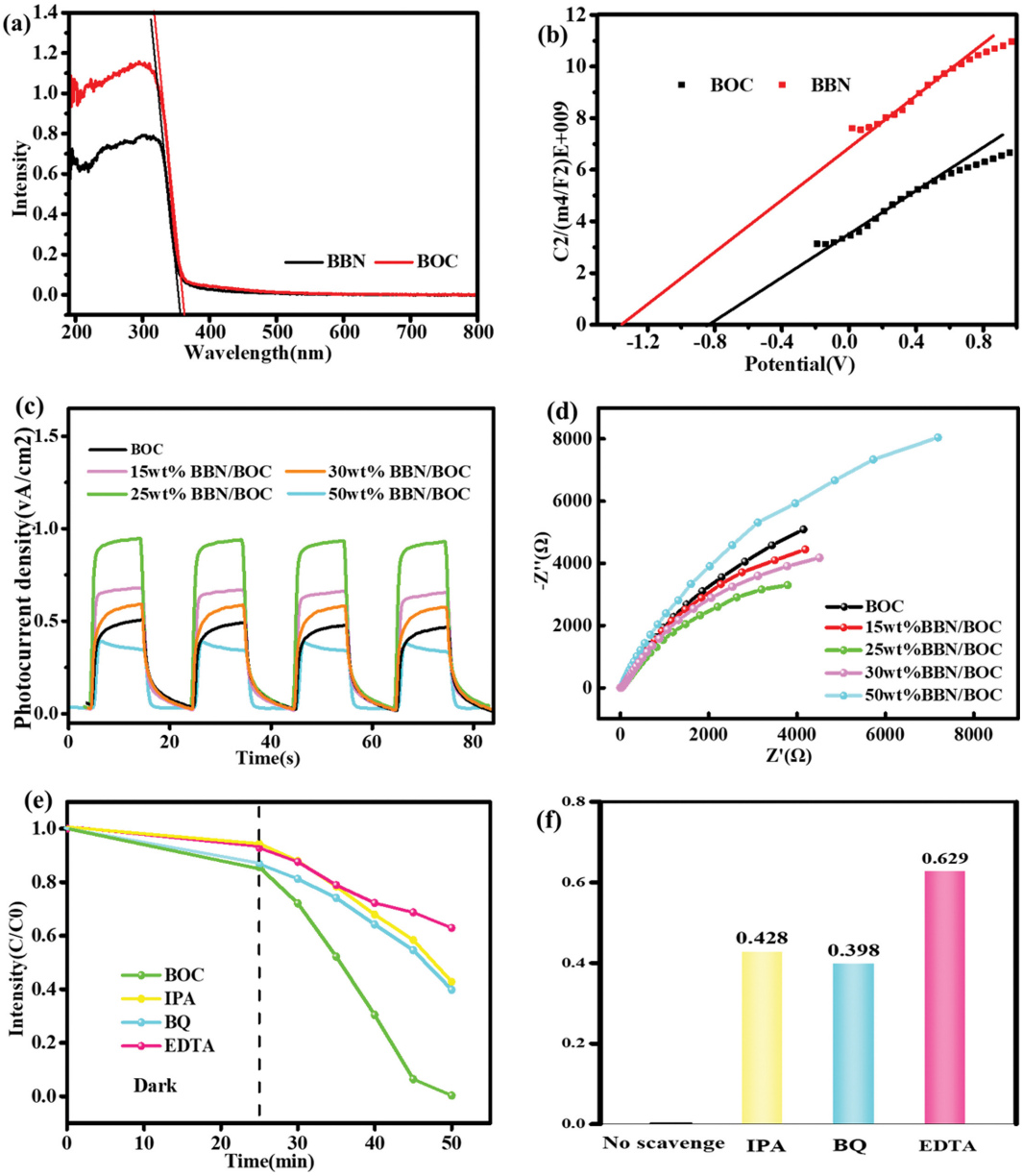

Fig. 5. The UV-vis of BOC and BBN (a)-(b), Transient photocurrent response (c), and Nyquist plots of EIS (d) of samples, the trapping experiments over 25wt%BBN/BOC composite (e)-(f).

used as a scavenger of $\cdot O_2^-$ and ·OH, the removal rate was importantly enhanced. Hence, we concluded that the h^+ of 25 wt%BBN/BOC composite took the dominating role in the photocatalytic degradation process, and the $\cdot O_2^-$ and ·OH acted as cofactors.

Based on the above experimental results and analysis, the photocatalytic mechanism of BBN/BOC composites was supposed, as shown in Fig. 6. Under simulated sunlight irradiation, the e^- of BOC and BBN are excited from the VB translates to the CB, leaving photo-generated h^+ in their corresponding VB. Benefiting from the existence of heterojunction, the h^+ generated in BOC migrates to the VB of BBN for its higher position than that of BBN, converting H_2O and OH^- to ·OH. In addition, the photogenerated e^- from BBN migrate to the CB of BOC simultaneously, converting O_2 to $\cdot O^{2-}$. In this way, the composite rate of photogenerated e^- and h^+ is reduced to a large extent, thus improving the photocatalytic degradation efficiency. More importantly, these active factors with strong REDOX capacity can degrade RhB, which is refractory to degrade, into small molecules like water and carbon dioxidethe, so as to achieve the purpose of sewage purification.

CONCLUSION

The BBN/BOC heterojunction was synthesized by a facile two-step hydrothermal approach. Benefiting from the interface electric field at the heterointerface, 25 wt%BBN/BOC composite possess outstanding charge separation and mobility properties. Also, the BOC flower-like structure decorated by BBN particles could provide more active sites for the reaction. Contributing to those advan-

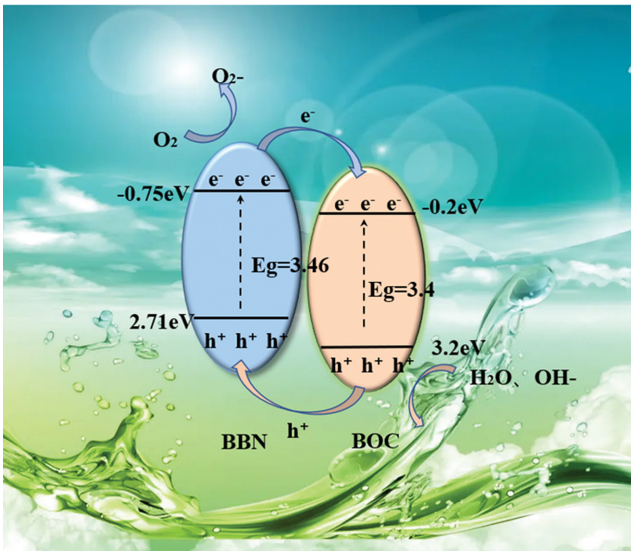

Fig. 6. Schematic illustration of the possible mechanism for the elimination of RhB over the BBN/BOC composite under simulated solar light irradiation.

tages, the photocatalytic degradation of RhB of 25 wt%BBN/BOC composite was enhanced to a large extent more than pure BOC and BBN, which could achieve 99.97% in 25 min under simulated sunlight irradiation.

ACKNOWLEDGEMENTS

This work was supported by the Natural Science Foundation of Fujian Province (2020J01833), the Fujian Engineering Research Center of New Chinese lacquer Material (No. 323030030702), and we humbly acknowledge international funding provided by Fujian Agriculture and Forestry University (No. KXB16001A).

CONFLICT OF INTEREST

The authors have no conflict of interest with regards to the submission and publication of this article.

SUPPORTING INFORMATION

Additional information as noted in the text. This information is available via the Internet at http://www.springer.com/chemistry/journal/11814.

REFERENCES

1. H. A. Qdais and H. Moussa, *Desalination*, **164**, 105 (2004).
2. L. Gao, X. Li, J. Zhao, X. Zhang, X. Zhang and H. Yu, *J. Phys. Chem. Solids*, **108**, 30 (2017).
3. L. Liang, J. Cao, H. Lin, X. Guo, M. Zhang and S. Chen, *Appl. Surf. Sci.*, **414**, 365 (2017).
4. H. Liu, P. Chen, X. Yuan, Y. Zhang, H. Huang, L. Wang and F. Dong, *Cuihua Xuebao/Chin. J. Catal.*, **40**, 620 (2019).
5. J. Xu, K. K. Wang, T. Liu, Y. Peng and B. G. Xu, *Crystengcomm*, **34**, 4945 (2017).
6. J. Zhong, J. Li, S. Huang, C. Cheng, W. Yuan, M. Li and J. Ding, *Mater. Res. Bull.*, **77**, 185 (2016).
7. Y. Qiu and J. Zhou, *Chemosphere*, **214**, 319 (2019).
8. H. Lu, Q. Hao, T. Chen, L. Zhang, D. Chen, C. Ma, W. Yao and Y. Zhu, *Appl. Catal. B: Environ.*, **237**, 59 (2018).
9. J. Kong, Z. Rui, X. Wang, H. Ji and Y. Tong, *Chem. Eng. J.*, **302**, 552 (2016).
10. J. Zai, F. Cao, N. Liang, K. Yu, Y. Tian, H. Sun and X. Qian, *J. Hazard. Mater.*, **321**, 464 (2017).
11. P. Chen, H. Liu, Y. Sun, J. Li, W. Cui, L. Wang, W. Zhang, X. Yuan, Z. Wang, Y. Zhang and F. Dong, *Appl. Catal. B: Environ.*, **264**, 118545 (2020).
12. N. Tavker and M. Sharma, *J. Environ. Manage.*, **255**, 109906 (2020).
13. L. Qiang, G. Li, X. Hu and W. Tian, *J. Photochem. Photobiol. A: Chem.*, **367**, 375 (2018).
14. S. Sun, X. Jiang, W. Xiao, Y. Jiang, W. Zhou, I. Lawan, M. Zhang, Z. N. Garba, L. Wang and Z. Yuan, *Mater. Lett.*, **276**, 128199 (2020).
15. J. Li, X. Wu, Z. Wan, H. Chen and G. Zhang, *Appl. Catal. B: Environ.*, **243**, 667 (2019).
16. H. Liu, P. Chen, X. Yuan, Y. Zhang, H. Huang, L. Wang and F. Dong, *Cuihua Xuebao/Chin. J. Catal.*, **40**, 620 (2019).
17. C. Lai, F. Xu, M. Zhang, B. Li, S. Liu, H. Yi, L. Li, L. Qin, X. Liu, Y. Fu, N. An, H. Yang, X. Huo, X. Yang and H. Yan, *J. Colloid Interface Sci.*, **588**, 283 (2021).
18. Z. Zhao, Y. Zhou, F. Wang, K. Zhang, S. Yu and K. Cao, *ACS Appl. Mater. Interfaces*, **7**, 730 (2015).
19. M. Sun, X. Wang, Z. Chen, M. Muruganantha, Y. Chen and Y. Zhang, *Appl. Catal. B: Environ.*, **273**, 119061 (2020).
20. W. Hou, H. Xu, Y. Cai, Z. Zou, D. Li and D. Xia, *Appl. Surf. Sci.*, **530**, 147218 (2020).
21. W. Zhang, J. Fu, Y. Wang, X. Zhang and J. Li, *J. Phys. Chem. Solids*, **127**, 19 (2019).
22. L. Man, Q. Xu, W. Li, W. Chen, W. Zheng and D. K. Ma, *Appl. Surf. Sci.*, **512**, 145647 (2020).
23. Y. R. Lv, R. K. He, Z. Y. Chen, X. Li and Y. H. Xu, *J. Colloid Interface Sci.*, **560**, 293 (2020).
24. X. Liang, J. Zhao, T. Wang, Z. Zhang, M. Qu and C. Wang, *ACS Appl. Mater. Interfaces*, **13**, 33034 (2021).
25. Y. Si, J. Li, J. Zhong, J. Zeng, S. Huang, W. Yuan, M. Li and J. Ding, *Curr. Appl. Phys.*, **16**, 240 (2016).
26. X. Hu, H. Zhao, Y. Liang, F. Chen, J. Li and R. Chen, *Chemosphere*, **264**, 128434 (2021).
27. Y. Ma, Q. Han, X. Wang and J. Zhu, *Mater. Res. Bull.*, **101**, 272 (2018).
28. P. Zhang, Y. Rao, Y. Huang, M. Chen, T. Huang, W. Ho, S. Lee, J. Zhong and J. Cao, *Chem. Eng. J.*, **420**, 129814 (2021).
29. X. Wei, M. U. Akbar, A. Raza and G. Li, *Nanoscale Adv.*, **3**, 3353 (2021).

Supporting Information

Facile construction of a $Bi_6O_6(OH)_3(NO_3)_3 \cdot 1.5H_2O/Bi_2O_2CO_3$ heterojunction with enhanced photocatalytic degradation activity

Huilan Ye*, Yiting Wu*, Ziqing Zhong*, Shichang Sun*, Jia Chen, Weiming Zhou*, Ibrahim Lawan***, Liwei Wang****,†, and Zhanhui Yuan*,†**

*College of Materials Engineering, Fujian Agriculture and Forestry University, Fuzhou, 350002, China
**College of Mechanical and Electrical Engineering, Fujian Agriculture and Forestry University, Fuzhou, 350002, China
***Department of Agricultural and Environmental Engineering, Bayero University Kano, Nigeria
****Ocean College, Minjiang University, Fuzhou 350108, China
(*Received 23 June 2021 • Revised 29 September 2021 • Accepted 6 October 2021*)

Table S1. The recent similar composites for photocatalytic dye degradation

Type of catalysis	Organic pollutant	Light source	Reaction condition	Photocatalytic performance	Ref.
$(BiO)_2CO_3/BiOBr$	RHB (25 mg/L)	300 W Xe	Visible light	99.80% in 60 min	[1]
$Bi_2O_2CO_3/BiOBr$	RHB (10 mg/L) 40 ml	400 W Xe	Visible light	94% in 20 min	[2]
$(BiO)_2CO_3/BiOI$	RHB (10 mg/L) 50 ml	500 W Xe	UV-visible light	81.3% in 30 min	[3]
$Bi_6O_6(OH)_3(NO_3)_3 \cdot 1.5H_2O/g\text{-}C_3N_4$	RhB (10 mg/ L)	500 W Xe	Visible light	88% in 120 min	[4]
$Bi_6O_6(OH)_3(NO_3)_3 \cdot 1.5H_2O/Bi_2WO_6$	RhB (10^{-5} M)	500 W Xe	UV-visible light	90% in 30 min	[5]
$Bi_6O_6(OH)_3(NO_3)_3 \cdot 1.5H_2O/BiOCl_{0.2}Br_{0.8}$	RhB (10 mg/L)	500 W Xe	UV-visible light	91% in 60 min	[6]
$Bi_6O_6(OH)_3(NO_3)_3 \cdot 1.5H_2O/Bi_2O_2CO_3$	RhB (10 mg/L)	250 W Xe	UV-visible light	99% in 25 min	This work

REFERENCES

1. L. Gao, X. Li, J. Zhao and X. Zhang, *J. Phys. Chem. Solids*, **108**, 30 (2017).
2. F. Qiu, W. Li, F. Wang, H. Li, X. Liu and C. Ren, *Colloids Surf. A: Physicochem. Eng. Aspects*, **517**, 25 (2017).
3. Y. Si, J. Li, J. Zhong and J. Zeng, *Curr. Appl. Phys.*, **16**, 240 (2016).
4. Y. Ma, Q. Han, X. Wang and J. Zhu, *Mater. Res. Bull.*, **101**, 272 (2018).
5. Y. Cui, L. M. Yang, G. Y. Zhang and Y. Feng, *Catal. Commun.*, **59**, 83 (2015).
6. L. Qiang, G. Li, X. Hu and W. Tian, *J. Photochem. Photobiol. A: Chem.*, **367**, 375 (2018).